CORROSION SCIENCE AND TECHNOLOGY, Vol.5, No.2(2006), pp.52~61

Tribological Behavior of Multilayered WC-$Ti_{1-x}Al_xN$ Coatings Deposited by Cathodic Arc Deposition Process on High Speed Steel

† Jung Gu Kim and Woon Suk Hwang[1]

Department of Advanced Materials and Engineering, Sungkyunkwan University
300 Chunchun-Dong, Jangan-Gu, Suwon, 440-746, Korea
[1]School of Materials Science and Engineering, Inha University
253 Yonghyun-Dong, Incheon 452-752, Korea

Recently, much of the current development in surface modification engineering are focused on multilayered coatings. Multilayered coatings have the potential to improve the tribological properties. Four different multilayered coatings were deposited on AISI D2 steel. The prepared samples are designed as WC-$Ti_{0.6}Al_{0.4}N$, WC-$Ti_{0.53}Al_{0.47}N$, WC-$Ti_{0.5}Al_{0.5}N$ and WC-$Ti_{0.43}Al_{0.57}N$. The multilayered coatings were investigated with respect to coating surface and cross-sectional morphology, roughness, adhesion, hardness, porosity and tribological behavior. Especially, wear tests of four multilayered coatings were performed by using a ball-on-disc configuration with a linear sliding speed of 0.017 m/sec, 5.38 N load. The tests were carried out at room temperature in air by employing AISI 52100 steel ball (H_R = 66) having a diameter of 10 mm. The surface morphology, and topography of the wear scars of samples and balls have been determined by using scanning electron spectroscopy (SEM). Results have showed an improved wear resistance of the WC-$Ti_{1-x}Al_xN$ coatings with increasing of Al concentration. WC-$Ti_{0.43}Al_{0.57}N$ coating with the lower surface roughness and porosity with good adhesion enhanced wear resistance.

Keywords *: Tribological, Porosity, Adhesion, Wear scar, Oxide layer, Potentiodynamic polarization test*

1. Introduction

The development of 'clean' technologies, in all spheres of industrial manufacturing, is an essential task required today and initiated by environmental laws and programs of countries around the world. In accordance with new environmental limitations, nearly all coatings produced by physical vapor deposition (PVD) find many functional and decorative applications. Especially, the development of tribological PVD coatings used to extend the life of cutting tools, dies, punches, and in applications such as ball bearings to minimize wear has been focused on multilayered coatings.[1)] A possible approach is the replacement of single layered coatings with mulitlayered coatings. Such coatings are obtained by alternately depositing mechanically different materials. The multilayered structure will act as a crack inhibitor and thereby increase the coating fracture resistance.[2)] Generally, these multilayers include two zones - the compound layer which is responsible for improving the tribological, electrochemical properties and the diffusion layer which often provides additional benefits including enhanced fatigue properties.[3)-4)]

Titanium nitride (TiN) coatings are widely used to increase the performance of tool steels. When working at temperature above 500°C, TiN tends to oxidize. This behavior leads to decreased mechanical and tribological properties of the coatings. A solution to this problem is to add Al contents to the TiN, forming TiAlN coatings. Recently, WC-$Ti_{1-x}Al_xN$ coatings with superior oxidation and tribological resistance have been developed. In this work a new PVD coating, consists of two metals, WC-Ti and WC-$Ti_{1-x}Al_xN$, combined into a multilayered coating structure has been evaluated.

The aim of this work was to evaluate the effect on aluminum concentration on the tribological behavior of WC-$Ti_{1-x}Al_xN$ coatings and to determine the relationships between the tribological properties and the mechanical characteristics of coatings.

† Corresponding author: kimjg@skku.ac.kr

2. Experimental

2.1 Material preparation and coating deposition

To deposit the multilayered WC-$Ti_{1-x}Al_xN$ coatings the following procedure was adopted. WC-$Ti_{1-x}Al_xN$ coatings were deposited on Si-wafer and AISI D2 steel by cathodic arc deposition. The nominal chemical compositions of the substrate were (wt.%) : 5.0 Cr, 1.3 Mo, 1.0 V, 1.0 Si, 0.5 Mn, 0.37 C, 0.03 P, 0.03 S and 90.77 Fe. All samples were ground to 2000 grit on side face, cleaned in distilled water and dried with ethyl alcohol followed by warm air blow-dryer prior to coating deposition. The substrates were axially attached to a jig holder inside chamber to offer a flat disc-shaped surface of 0.78 cm^2 area. The distance between the substrate and the target was 200 mm. Si wafer was used as the substrate for investigating the cross-sectional morphology.

Three circular Ti cathodes were installed on one side of the chamber wall and three circular WC cathodes were attached on the other side. Two Al cathodes were installed between the Ti cathodes. Prior to coating, the substrate was subjected to Ti ion etching. For the improvement of adhesion between the substrate and multilayered coating, a 100 nm thick Ti/TiN interlayer was deposited. An improvement in the corrosion resistance can be obtained with a better coating adhesion. For the reduction of film stress, periodic layers (bi-layer thickness : 20 nm) of multilayer WC-$Ti_{1-x}Al_xN$ and a buffer layer of WC-Ti were deposited by selective arc discharge and modulating N_2 flow, with the substrate biased at -100 V. The chamber was evacuated to a pressure of 0.5333×10^{-3} Pa and the deposition temperature was maintained using a radiant heater. A rotation substrate holder was placed at the center of the chamber and rotated with a rotation frequency of 7 rpm. A detail of coating structure is presented in Fig. 1. A total coating thickness of 2.1 ㎛ was aimed at in all cases. Field emission gun scanning electron microscopy (FEG-SEM) was utilized to measure the coating thickness.

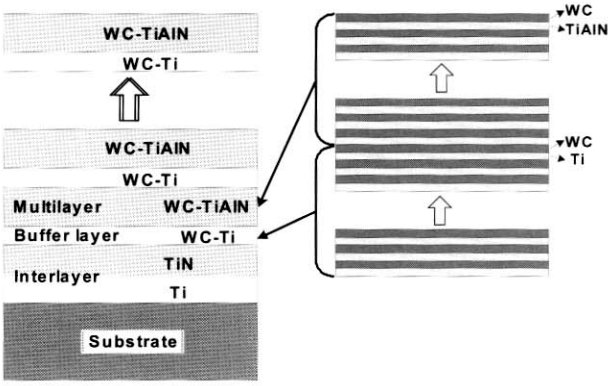

Fig. 1. Schematic diagram of the structure of multilayered WC-$Ti_{1-x}Al_xN$ coatings.

2.2 Evaluation methods

The porosity was determined through the use of electrochemical methods from four kinds of protective coatings. Potentiodynamic polarization curves were obtained using an EG&G PAR 273A potentiostat in a 3.5 wt.% NaCl electrolyte at room temperature. All tests were tested in a conventional three-electrode electrochemical cell. A saturated calomel and a pure graphite were used for reference electrode and counter electrode. The potential of the electrode was swept at a rate of 0.166 mV/sec from the initial potential of -250 mV versus E_{corr} to the final potential of 1000 mV.

Combination of the equation of Matthews et al.[5] with the electrochemical results gives the porosity.

$$F = \frac{R_{pm(substrate)}}{R_{p(coating-substrate)}} \times 10^{-|\triangle E_{corr}/\beta_a|} \quad (1)$$

Where F is the total coating porosity, R_{pm} the polarization resistance of the substrate, R_p the measured polarization resistance of the coating. ΔE_{corr} the difference of corrosion potential between coating and substrate, and β_a the anodic Tafel slope of the substrate.

A scratch tester was used to determine a critical load (L_c). A loading rate 10 N/sec (total range 0 - 100N) was utilized. The applied load is increased continuously until the detachment of the coating. The critical load is defined as the smallest load at which the coating is damaged.

The coating hardness was measured using a Rockwell hardness tester with a load of 25 g. Ball-on-disc configuration tribometer was employed to investigate the wear behavior of the WC-$Ti_{1-x}Al_xN$ coating. The tests were carried out by employing an AISI 52100 steel ball having a diameter of 10 mm. Steel balls were cleaned in an ultrasonic acetone bath before the tests. The wear experiments were performed in air, without lubrication, at a temperature of 298 K. A load of 5.38 N and a sliding velocity of 0.017 m/sec were used. Sliding distance was kept at 155.6 m. The radius of the traveling circle of the ball-on-disc was 11 mm. The surface morphology of the coated sample and the topography of the wear scar have been analyzed by using SEM. The wear mechanism was determined by using SEM coupled with EDS.

The wear volume of the ball (V) was calculated by approximating the worn volume to a spherical cap. The diameter (d) of the spherical cap produced on the specimen by abrasion was measured with a calibrated optical microscope. By assuming that the height of the cap is much

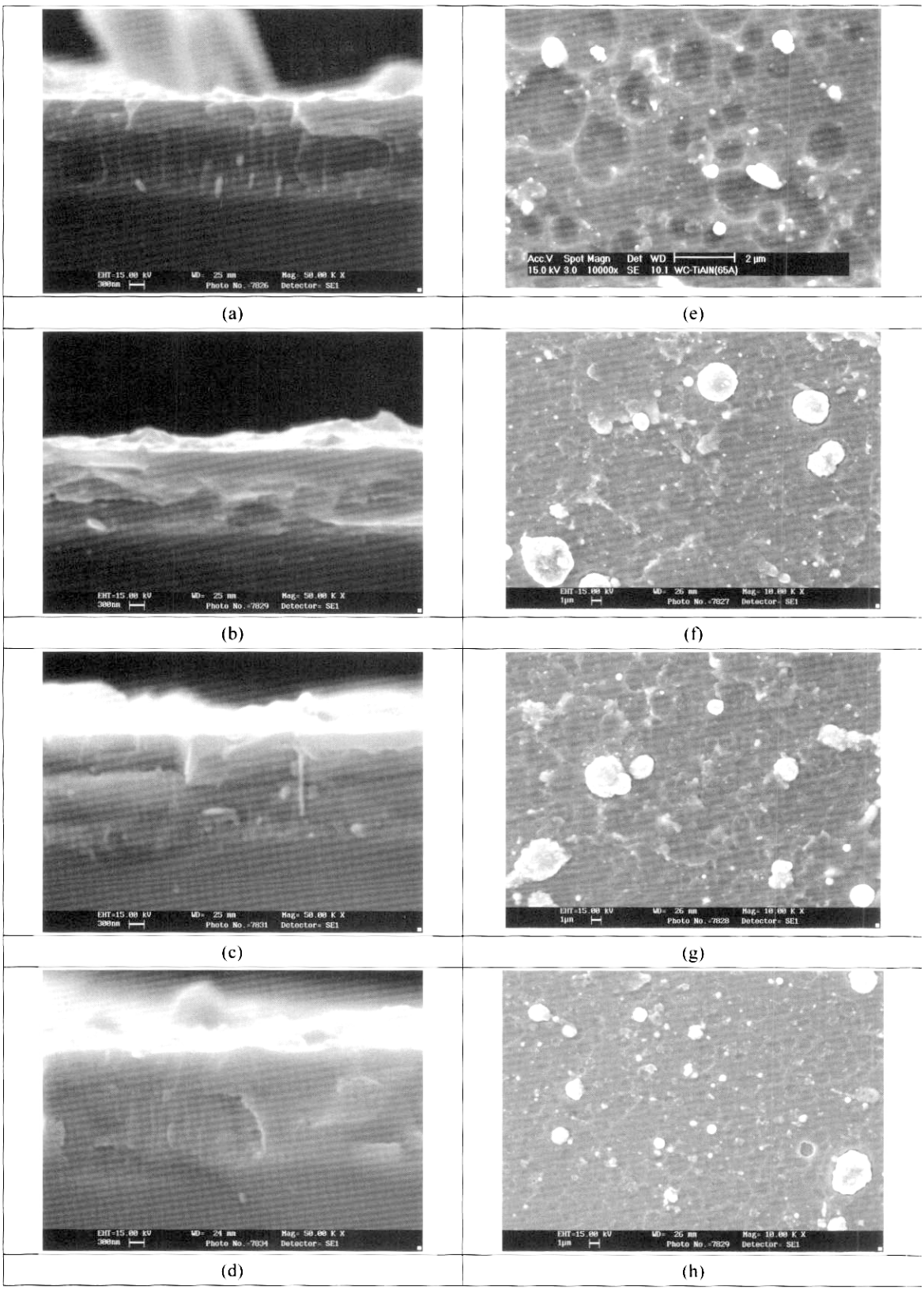

Fig. 2. SEM images of a surface and cross-section; (a,e) WC-$Ti_{0.6}Al_{0.4}N$ (b,f) WC-$Ti_{0.53}Al_{0.47}N$ (c,g) WC-$Ti_{0.5}Al_{0.5}N$ (d,h) WC-$Ti_{0.43}Al_{0.57}N$.

smaller than the ball radius (R), the wear volume can be calculated by :

$$V=\frac{\pi d^4}{64R} \quad (2)$$

where d is the wear scar diameter (d≪R).[6]

3. Results and discussion

3.1 Surface and cross-sectional morphology

The chemical compositions of the multilayered coatings were measured using EDS. The prepared specimens are designated as WC-$Ti_{0.6}Al_{0.4}N$, WC-$Ti_{0.53}Al_{0.47}N$, WC-$Ti_{0.5}Al_{0.5}N$ and WC-$Ti_{0.43}Al_{0.57}N$. Fig. 2(a-d) show cross-sectional SEM images of the WC-$Ti_{1-x}Al_xN$ coatings on Si-wafer substrate. A majority of the coatings exhibited a very dense and columnar structure for the cross-sectional morphology. Also, it has been found that the amplitude of the surface irregularities (small craters and droplets) decreases with increasing aluminum content, as shown in Fig. 2(e-h). This is attributed to a decrease in the resistance between the coating and the steel ball and to a decrease in the wear volume of counter part (the steel ball). Surface morphologies were determined by the distribution of particles (mainly droplets). It is believed that these particles may act as stress concentrator and decrease the fracture resistance of the coating.

The values obtained from the roughness measurement were represented in Table 1. As the aluminum concentration increases, the surface roughness R_a decreases.

3.2 Coating adhesion, hardness, and porosity rate

Fig. 3 and Table 1 show the acoustic emission signal and the measured critical load. For the WC-$Ti_{1-x}Al_xN$ coating, critical adhesion loads up to approximately 52N were obtained for the best samples (WC-$Ti_{0.5}Al_{0.5}N$ and WC-$Ti_{0.43}Al_{0.57}N$), while the mechanism responsible for the failure is directly related with spallation.

Table 1. Properties of WC-$Ti_{1-x}Al_xN$ coating deposited at different Al concentration.

Specimen	Roughness R_a (㎛)	Scratch test L_C (N)	Hardness H_R
Substrate			65
WC-$Ti_{0.6}Al_{0.4}N$	9.3	21.97	87.6
WC-$Ti_{0.53}Al_{0.47}N$	3.8	50.97	87.6
WC-$Ti_{0.5}Al_{0.5}N$	6.7	51.97	89.3
WC-$Ti_{0.43}Al_{0.57}N$	5.5	51.97	90.6

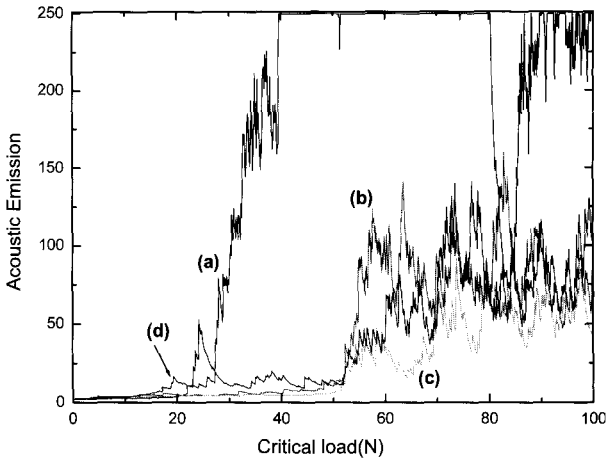

Fig. 3. Results of scratch adhesion tests for WC-$Ti_{1-x}Al_xN$ coatings; (a) WC-$Ti_{0.6}Al_{0.4}N$ (b) WC-$Ti_{0.53}Al_{0.47}N$ (c) WC-$Ti_{0.5}Al_{0.5}N$ (d) WC-$Ti_{0.43}Al_{0.57}N$.

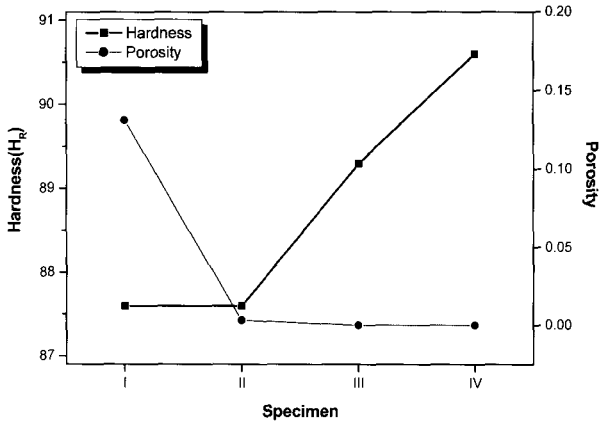

Fig. 4. Hardness and porosity of WC-$Ti_{1-x}Al_xN$ coatings; (I) WC-$Ti_{0.6}Al_{0.4}N$ (II) WC-$Ti_{0.53}Al_{0.47}N$ (III) WC-$Ti_{0.5}Al_{0.5}N$ (IV) WC-$Ti_{0.43}Al_{0.57}N$.

Also, the variation in hardness of the WC-$Ti_{1-x}Al_xN$ coatings as a function of the aluminum concentration of WC-$Ti_{1-x}Al_xN$ coating is presented in Table 1. The hardness is the average of three measurements. It was found that the value of hardness increased when the aluminum content increased.

The properties of adhesion and hardness are improved by multi-step surface pretreatments and by controlling the coating structure. Thus, it is an important to control the porosity in the coatings. The porosity was determined from the measured polarization resistance at a given potential. The porosity obtained by electrochemical method means the overall porosity including the open pore in the outer surface and the closed pore through the coating system. The electrochemical determination gives a porosity of 0.1310 for WC-$Ti_{0.6}Al_{0.4}N$, 0.0032 for WC-$Ti_{0.53}Al_{0.47}N$, 0.696×10^{-6} for WC-$Ti_{0.5}Al_{0.5}N$, and 0.001×10^{-6} for WC-

Table 2. Results of electrochemical experiments.

Specimen	E_{corr} (mV)	i_{corr} ($\mu A/cm^2$)	β_a (V/decade)	β_c (V/decade)	R_p ($\times 10^3$ Ωcm^2)	Porosity
Substrate	-541.9	14.69	0.096	0.2231	1.988	
WC-$Ti_{0.6}Al_{0.4}N$	-515.9	5.084	0.1351	0.3222	8.1404	0.1310
WC-$Ti_{0.53}Al_{0.47}N$	-384.8	1.471	0.0884	0.1	13.868	0.0032
WC-$Ti_{0.5}Al_{0.5}N$	-162.1	0.267	0.3773	0.3984	315.72	0.696×10^{-6}
WC-$Ti_{0.43}Al_{0.57}N$	-34.6	0.0009	0.2904	0.2623	6449.3	0.001×10^{-6}

$Ti_{0.43}Al_{0.57}N$, as shown in Table 2. The porosity value obtained for WC-$Ti_{0.6}Al_{0.4}N$ coating is much higher than the others. The relationship between hardness and porosity was shown in Fig. 4. Thus, the increase of the aluminum content led to a substantial decrease in porosity. WC-$Ti_{1-x}Al_xN$ coatings show an increase in hardness with increasing aluminum concentration and decreasing the porosity. This may be due to the fact that the coating with a lower porosity has a denser structure, which is more resistant to plastic deformation. Hard materials with a lower porosity generally wear less than soft materials under the same frictional conditions.[7]

3.3 Wear measurement

The friction coefficients as a function of sliding time are presented in Fig. 5. As one can observe in this figure, the friction coefficient value of WC-$Ti_{0.6}Al_{0.4}N$ disc was higher than others. At the beginning of the test, the friction coefficient increased rapidly, reaching a maximum value of 0.39 before 1,400 sec of sliding time. It was thought that the high friction coefficient obtained was due to an increase in the asperity interactions, i.e., asperities on the coating surface work as abrasive asperities. Local pressure at contacting peaks of surface asperities may be sufficiently high to cause significant plastic deformation.[8] This leads to the formation of connections among asperity peaks and increasing the area of contact with progressing deformation of the material. A steady value of 0.39 remained until nearly 1,400 sec of sliding time when a sudden drop to 0.3 occurred. This value was maintained nearly constant. This drop in friction coefficient value might be due to changed mating surface compared to that existing at the beginning of the test. Diameter of wear scar on WC-$Ti_{0.6}Al_{0.4}N$ coating was much wider than other coatings as seen from the values given in Table 3. WC-$Ti_{0.43}Al_{0.57}N$

Table 3. Wear volume of steel ball after wear test against WC-$Ti_{1-x}Al_xN$ coatings.

Specimen	Diameter of wear scar (mm)	Wear volume ($\times10^{-6}$ mm^3)
WC-$Ti_{0.6}Al_{0.4}N$	1.1385	16.5
WC-$Ti_{0.53}Al_{0.47}N$	0.6920	2.25
WC-$Ti_{0.5}Al_{0.5}N$	0.7395	2.93
WC-$Ti_{0.43}Al_{0.57}N$	0.6530	1.78

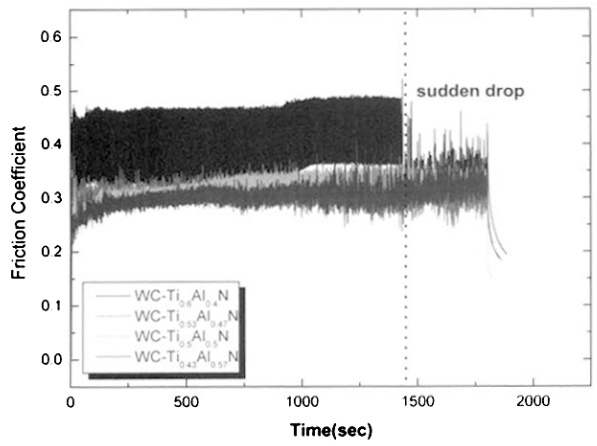

Fig. 5. Typical recording of friction coefficient vs. test time when sliding a steel ball against the multilayered coatings; (a) WC-$Ti_{0.6}Al_{0.4}N$ (b) WC-$Ti_{0.53}Al_{0.47}N$ (c) WC-$Ti_{0.5}Al_{0.5}N$ (d) WC-$Ti_{0.43}Al_{0.57}N$.

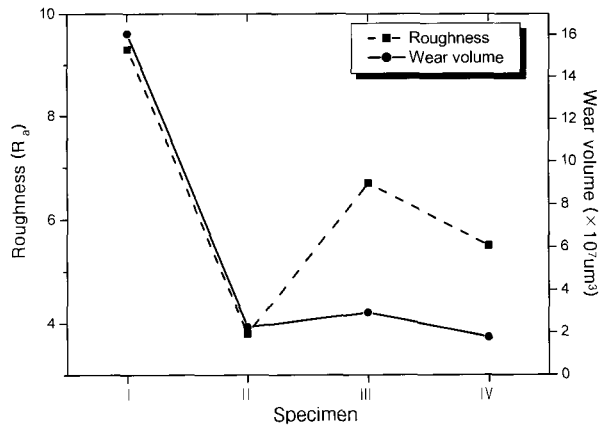

Fig. 6. Roughness of coated steels and wear volume of steel balls; (I) WC-$Ti_{0.6}Al_{0.4}N$, (II) WC-$Ti_{0.53}Al_{0.47}N$, (III) WC-$Ti_{0.5}Al_{0.5}N$, (IV) WC-$Ti_{0.43}Al_{0.57}N$.

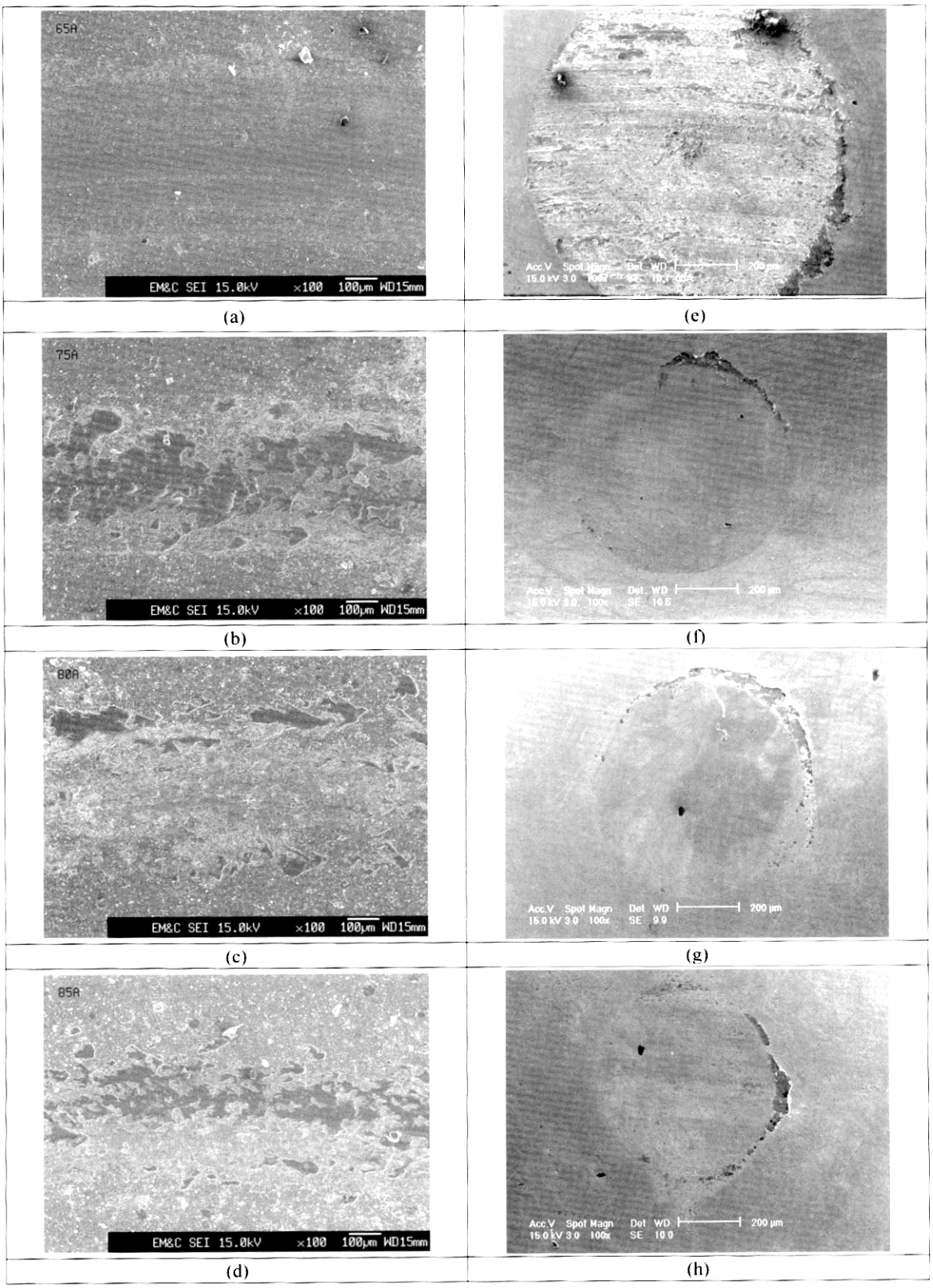

Fig. 7. Scanning electron micrographs showing topography of the WC-$Ti_{1-x}Al_xN$ coatings and the wear debris on the wear track; (a-d) the worn surface, and (e-h) the steel ball.
((a)WC-$Ti_{0.6}Al_{0.4}N$, (b) WC-$Ti_{0.53}Al_{0.47}N$, (c) WC-$Ti_{0.5}Al_{0.5}N$, (d) WC-$Ti_{0.43}Al_{0.57}N$)

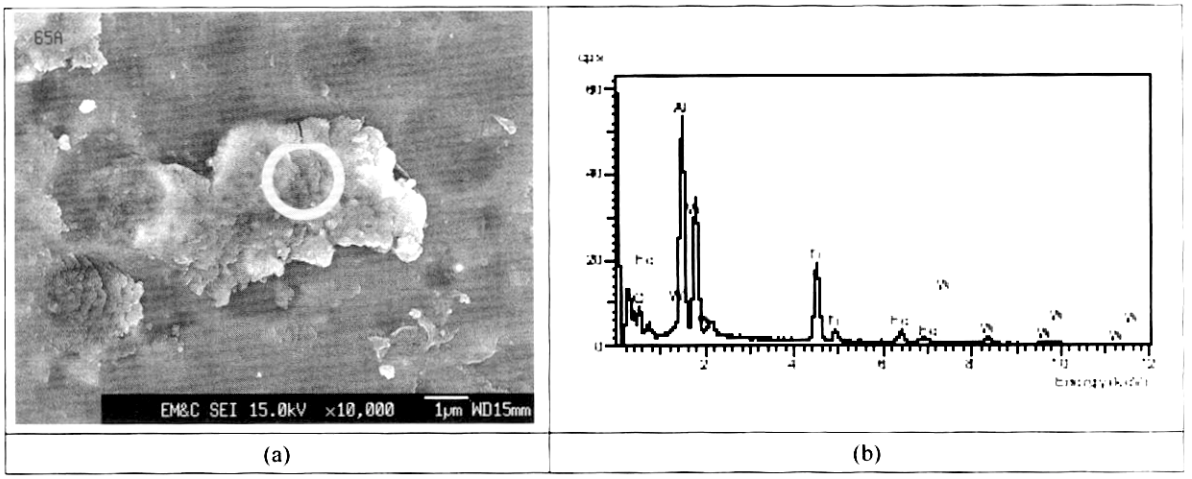

(a) (b)

Fig. 8. Representative micrographs of the wear debris of WC-$Ti_{0.6}Al_{0.4}N$ and EDS analysis of wear debris (circular point).

coating with a lower width of wear scar has superior sliding wear resistance.

Table 3 summarizes the wear diameter and wear volume measured on the steel balls used in the tests. The wear volume of counter-part (steel ball), when interacting with the four different types of multilayers, decreases with increasing aluminum content and with decreasing surface roughness in the coatings. This is represented in Fig. 6.

SEM morphologies of the wear scars produced on multilayered coatings and corresponding ball steels are represented in Fig. 7. The surface of the coated steels, except for WC-$Ti_{0.6}Al_{0.4}N$ (Fig. 7(a)), exhibits pronounced wear grooves with features of small particles, as shown in Fig. 7(b-d). This is due to the formation of oxide layer which is soft abrasive wear debris. Especially, the SEM images of the wear tracks on the WC-$Ti_{1-x}Al_xN$ coating show powder like asperities which are broken off from the coating surface. Debris formation of this type might enhance the wear. Whereas WC-$Ti_{0.6}Al_{0.4}N$ coating has the wear debris, which is getting smeared and deformed under the sliding steel ball (Fig. 8(a)). Large metal transfer from steel ball onto the coatings was detected. The EDS analysis of the wear debris revealed aluminum, iron, and oxygen elements, as shown in Fig. 8(b).[9-11] This is evident from the X-ray maps of the coating corresponding to aluminum and oxygen distribution as shown in Fig. 9, respectively. All surfaces except for WC-$Ti_{0.6}Al_{0.4}N$ coating have an oxidized surface. Usually, oxides are known to possess friction-reducing capabilities due to their relative softness.

4. Conclusions

1) For the WC-$Ti_{1-x}Al_xN$ coatings, the increase of the aluminum content led to a substantial decrease in porosity. This may led to a denser structure, which is more resistant to plastic deformation, and an increase in hardness and adhesion.

2) An increase in the asperity interactions coupled with the simultaneous production of hard abrasive particles results in a high friction coefficient value. The friction coefficient value of WC-$Ti_{0.6}Al_{0.4}N$ coating was higher and its wear volume was much larger than those of other coatings.

3) From the EDS analysis, the surface of the coated steels except for WC-$Ti_{0.6}Al_{0.4}N$ coating was observed to have oxide layer, which is known to present friction-reducing capabilities due to their relative softness. It was concluded that the best resistance of WC-$Ti_{0.43}Al_{0.57}N$ to wear is due to its low surface roughness and porosity with good adhesion.

Acknowledgments

The authors are grateful for the support provided by the Korea Science and Engineering Foundation through the Center for Advanced Plasma Surface Technology at Sungkyunkwan University.

References

1. U. Wiklund, O. Wanstrand, M. Larsson, and S. Hongmark, *Wear* **236**, 88 (1999).
2. K.N. Andersen, E.J. Bienk, K.O. Schweitz, H. Reitz, J. Chevallier, P. Kringh ϕ j, and J. B ϕ ttiger, *Surface and Coatings Technology* **123**, 219 (2000).
3. Milton Ohring, The Materials Science of Thin Films, Academic Process, London, p. 574-579. (1991)
4. Y. Sun and T. Bell, *Materials and Science Engineering* **A140**, 419 (1991).

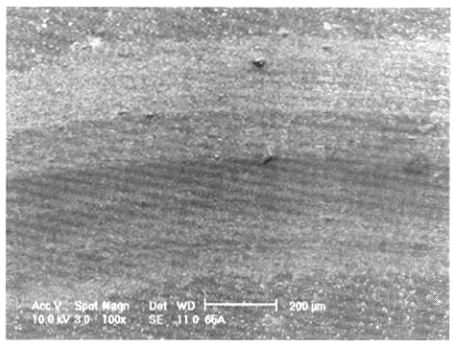

(i)

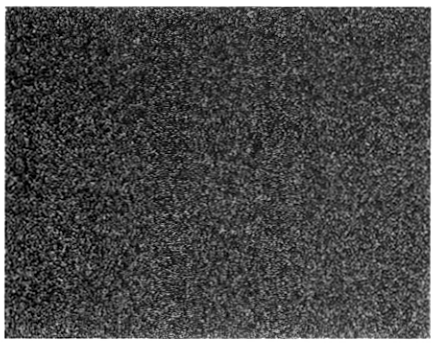

(a)

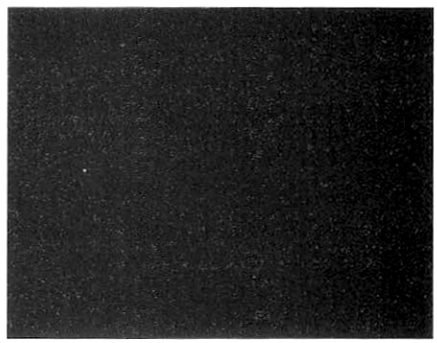

(b)

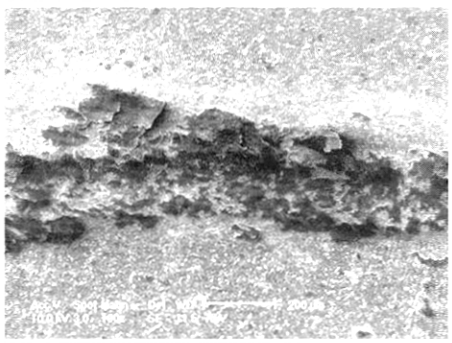

(ii)

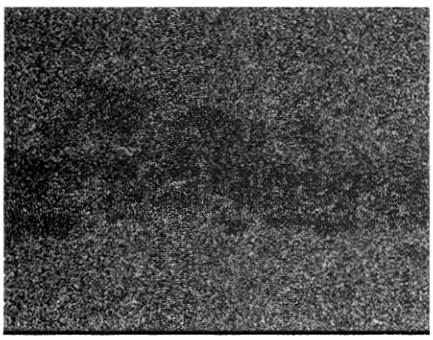

(a)

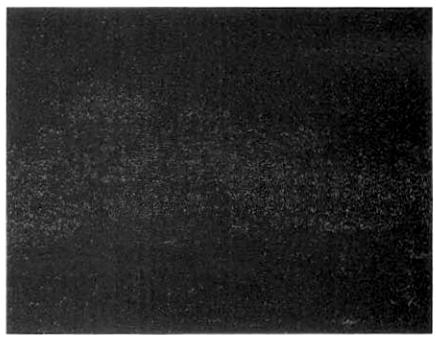

(b)

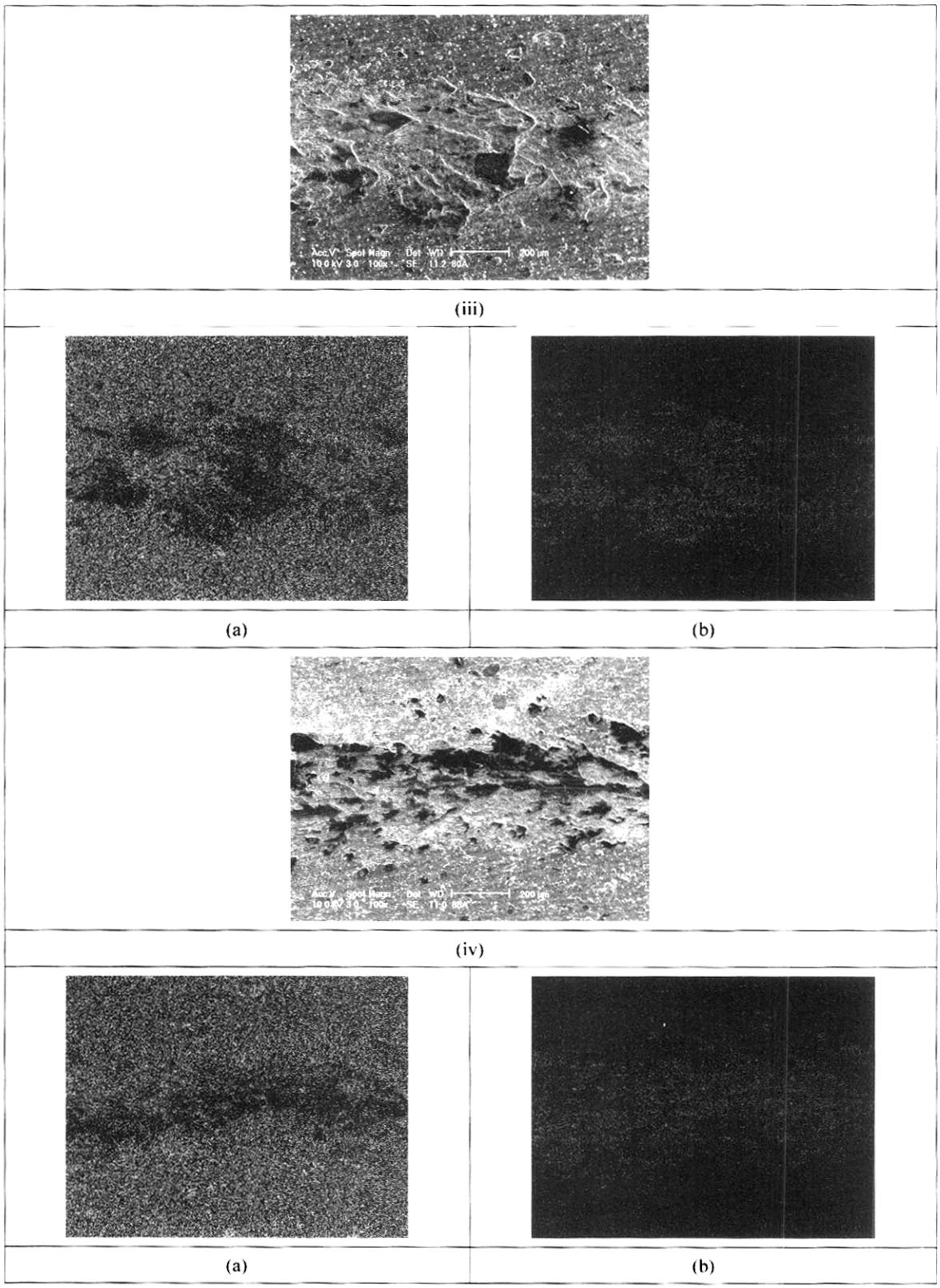

Fig. 9. SEM micrograph of the worn surface and corresponding X-ray elemental map of (a) Al and (b) O ; (i) WC-$Ti_{0.6}Al_{0.4}N$, (ii) WC-$Ti_{0.53}Al_{0.47}N$, (iii) WC-$Ti_{0.5}Al_{0.5}N$, (iv) WC-$Ti_{0.43}Al_{0.57}N$.

5. B. Matthes, E. Broszeit, J. Aromaa, H. Ronkainen, S.P. Hannula, A. Leyland, and A. Matthews, *Surface and Coatings Technology* **49**, 489 (1991).
6. U. Wiklund, O. Wanstrand, M. Larsson, and S. Hogmark, *Wear* **236**, 88 (1999).
7. K.H. Zum Gahr, *Tribol. Ser.* **10**, 174 (1987).
8. T. Burakowski and T. Wierzchon, Surface Engineering of Metals, CRC, New York, p. 140. (1999)
9. M. Larsson, M. Bromark, P. Hedenqvist, and S. Hogmark, *Surface and Coatings Technology* **91**, 43 (1997).
10. K. Kato, *Wear* **241**, 151 (2000).
11. M.H. Stain, A. Fragiel, S.P. Bruhl, J.N. Feugeas, and B.J. Gomez, *Thin Solid Films* **377-378**, 650 (2000).